

Boundary Shape Waveform Inversion for Two-Dimensional Basin Structure Using Three-Component Array Data of Plane Incident Wave with an Arbitrary Azimuth

by Shin Aoi, Tomotaka Iwata, Hiroyuki Fujiwara, and Kojiro Irikura

Abstract We extend a new waveform inversion scheme (Aoi *et al.*, 1995) for estimating underground structure with an irregular-shaped basement as a target to cases where plane waves with an arbitrary azimuth impinge on the structure, i.e., from a direction not necessarily perpendicular to the major axis of the structure. We proved the validity of this scheme by numerical experiments. We had already achieved the formulation and numerical experiments for the cases where an *SH* wave impinges on a 2D basin structure and had shown that we could estimate the entire basin structure with seismic waveforms from only a few surface stations by using whole waveforms that include the surface waves. However, when the epicenter is located out of the plane including the observation stations, even the cases of 2D structure cannot be treated as a simple 2D (*SH* or *P-SV*) problem because of the wave with an azimuth that is not 0° . Therefore, by dealing with 3D wave fields in the present study, we extend the inversion scheme in order to apply it to incident waves with an arbitrary azimuth. The differential seismograms, which represent the sensitivity of change in the waveform, show different patterns in three components, and we demonstrate that inversion with three components, compared with the inversion with only one of them, leads to a linearized equation system with a smaller condition number and a more stable computation. Furthermore, we detect certain parts that are estimated with much less difficulty than others, depending on the direction from which the incident wave impinged. In the latter case, we can estimate the entire structure by employing simultaneously several data from incident waves arriving from different directions. We thus demonstrate by numerical experiments that the extension of our inversion method to cases where the incident wave with an arbitrary azimuth impinges on the structure enables us to estimate with increased accuracy an underground structure under more general conditions of the epicenter locations.

Introduction

The detailed knowledge of an underground structure is very important, since the effects of a basin structure on the waveforms observed on the surface during an earthquake are considerable (e.g., Beck and Hall, 1986; Kawase and Aki, 1989; Hatayama *et al.*, 1995; Yamanaka *et al.*, 1989). In order to estimate the underground structure, many methods such as the refraction method and the reflection method have been proposed. However, there are certain difficulties in employing these methods. On one hand, with the refraction method, basically one can estimate only the structure that is located directly underneath the observation stations since the data used are only arrival times. The method does not allow us to perform a high-resolution analysis with data from a small number of observation stations. As to the reflection

method, on the other hand, the acquisition of records is extremely bothersome, and it requires artificial sources.

The inversion method, which uses the observed data to determine the causes of these data, has attracted the attention of many researchers in various fields because of its objectivity. For instance, tomography techniques are widely used to estimate underground structure in the field of seismology. However, a high-resolution analysis with the existing tomography technique requires numerous (several thousands or ten thousands) parameters. Thus, we proposed a new method to perform an inverse analysis of basin structure, which treats this problem as a domain/boundary inverse problem and requires a much smaller number of parameters (Aoi *et al.*, 1995). The domain/boundary inversion (Kubo,

1992) is a method to formulate the inverse problem by paying particular attention to the boundary shapes of several regions regarded as homogeneous. The method has already been used for more than 10 years in mechanical engineering (Barone and Caulk, 1982). For example, nondestructive inspection has been carried out to determine the shapes and locations of cavities or cracks in metal by using the data from measurements such as electric potentials on the surface (e.g., Nishimura and Kobayashi, 1991; Tanaka and Yamagawa, 1988; Kubo *et al.*, 1988). However, there are only a few applications of the domain/boundary inversion to seismology (Nowack and Braile, 1993; White, 1989).

Concerning the basin structure treated in the present study, since the impedance ratio is quite large between a hard basement with a high wave velocity and a soft sedimentary layer with a low wave velocity, we consider that each of them consists of an approximately homogeneous elastic medium. In our previous study, by choosing a boundary shape with large impedance ratio between the basement and the sedimentary layer as a target parameter, we performed successfully the inversion with only a few dozens of parameters. In this way, we carried out a formulation and numerical experiments for cases where an *SH* wave impinges on a 2D basin structure and showed the validity of this method and its robustness against noise. A significant difference between the inversion of underground structure in seismology and nondestructive inspection in mechanical engineering consists in a spatial mal-distribution of the observation stations as well as sources in the former. In more concrete terms, as to nondestructive inspection, one can determine the locations of receivers or sources in such a way that they encircle the object, while in most seismic observations, the measurements have to be made on the surface. The source locations are limited even for natural earthquakes as well as for artificial sources. Consequently, it was difficult to obtain sufficient data for carrying out the inversion. In order to reduce those difficulties, we decided to employ the waveform in-

version that uses as data the entire waveform instead of limited information such as the arrival times. We came to the conclusion that in cases where a plane *SH* wave impinges on a 2D double-layered structure, the use of surface waves generated secondarily by the structure enables us to estimate completely the entire structure with data from only a few observation stations (Aoi *et al.*, 1995).

In the present study, we will extend the previous method explained above to cases where the incident waves with an arbitrary azimuth impinge on the structure. We consider the incident wave from deep earthquakes approximately as a plane wave. When the epicenter is located out of the plane including the observation stations, the azimuth of the incident waves is not 0° , and the direction from which they impinge becomes oblique to the 2D structure. In these circumstances, even the cases of 2D structure cannot be treated as simple 2D (*SH* or *P-SV*) problems because of the incident wave with an oblique azimuth. Therefore, we will extend the inversion to the so-called 2.5D problem, which deals with 3D wave fields for 2D structures, so that we will be able to apply it to incident waves with an arbitrary azimuth (e.g., Fujiwara, 1996; Pedersen *et al.*, 1995; Pei and Papageorgiou, 1993). First of all, since three components in the differential seismograms show different patterns, it is preferable to carry out the inversion with three components than doing so with only one of them. This will be shown by the examination of condition number of linearized equation. Secondly, we will demonstrate that certain parts of the structure are easier to estimate than others, depending on the arrival direction of the incident wave. We will perform the inversions by using simultaneously the data from several incident waves arriving from different directions. Consequently, the extension of the present method to cases of incident waves with any azimuth impinging on the structure will enable us to perform the inversion with increased accuracy under more general conditions of the epicenter locations.

Configuration of the Model and the Incident Wave

Figure 1 shows our assumed 2D basin structure model, which lies along the *y* axis and consists of two homogeneous,

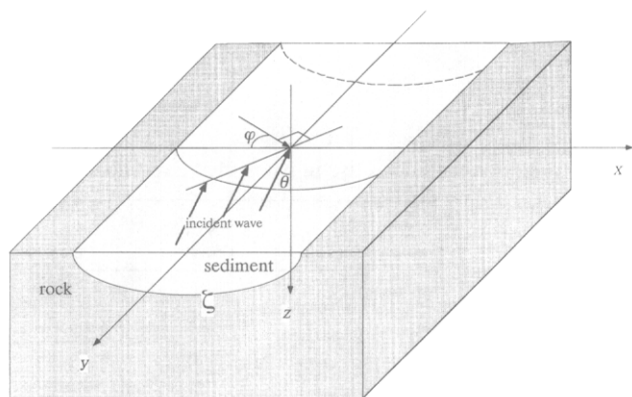


Figure 1. Configuration of the basin structure model and the incident wave. Plane wave with the incident angle θ and the azimuth ϕ impinges on the 2D basin structure model that lies along the *y* axis.

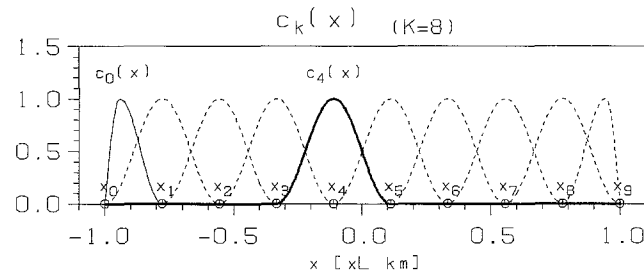


Figure 2. Examples of the space distribution of the weight function system $c_k(x)$ when $K = 8$. Thin and thick lines show the examples of $c_k(x)$ for $k = 0$ and $k = 4$, respectively.

isotropic, elastic media corresponding to a sedimentary layer and a basement. We will consider cases where the plane incident wave with an oblique azimuth impinges on this model. We define that the angle formed by the z axis and the wavenumber vector of the incident wave is the incident angle θ and that the angle formed by the negative x axis and the projection of the wavenumber vector on the xy plane is the azimuth φ .

When $\varphi = 0^\circ$, we can separate completely the SH and P - SV wave fields, which implies that it becomes a pure 2D problem. However, when $\varphi \neq 0^\circ$, we have to treat this as a 2.5D problem because of the reciprocal coupling of SH and P - SV wave fields. In this study, we carry out the waveform synthesis by using the boundary integral equation method formulated by Fujiwara (1996). By transforming the wave equation of the space-frequency domain into the wavenumber-frequency domain using a Fourier transformation only in the y direction, we obtain an equation that does not depend on y . This allows us to solve the problem of a 3D wave field for plane incident wave with an arbitrary azimuth within a reasonable computation time, which is only several times longer than that of a P - SV problem.

Function System and Parameters to Describe the Boundary Shape

In order to formulate a boundary shape to be estimated for an inverse problem, the boundary shape has to be discretized and described by several parameters. We denote this boundary shape $\zeta(x)$ as

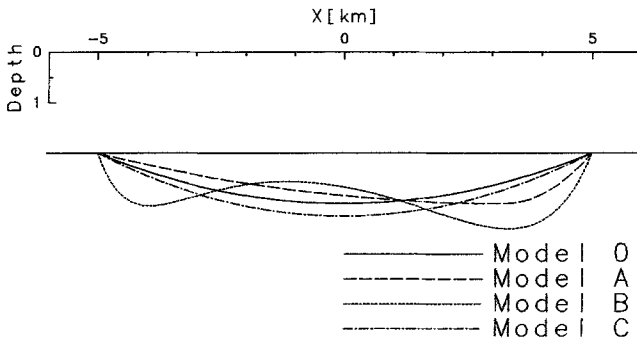


Figure 3. Basin structures of models 0, A, B, and C. The physical parameters are shown in Tables 1 and 2.

Table 1

Maximum Depths and Shapes of the Structure Models

| Model | Shape | Max. Depth (km) |
|----------------|-------------------------|-----------------|
| 0 | Parabola | 1.00 |
| A | Nonsymmetrical parabola | 1.00 |
| B | Plateau | 1.50 |
| C | Parabola | 1.25 |
| Width of basin | | 10 km |

$$\zeta(x) - \zeta^0(x) = \sum_{k=0}^{K+1} p_k \times c_k(x), \quad (1)$$

where $\zeta^0(x)$ denotes the boundary shape of the initial model. That is, the difference of depth between the initial and the target models is described by the expansion of the functions $c_k(x)$. We introduce the following as the function system $\{c_k(x) | k = 0, 1, \dots, K, K + 1\}$:

$$c_k(x) = \begin{cases} \frac{1}{2} \left\{ 1 + \cos \frac{\pi}{\Delta} (x - x_k) \right\} & \text{if } x_{k-1} \leq x \leq x_{k+1} \\ 0 & \text{otherwise} \end{cases}, \quad (2)$$

$(k = 1, 2, \dots, K)$

$$c_0(x) = \begin{cases} \sin \frac{\pi}{2\alpha\Delta} (L + x) & \text{if } -L \leq x \leq -L + \alpha\Delta \\ \frac{1}{2} \left\{ 1 + \cos \frac{\pi}{(1 - \alpha\Delta)} (L - \alpha\Delta + x) \right\} & \text{if } -L + \alpha\Delta \leq x \leq -L + \Delta, \\ 0 & \text{otherwise} \end{cases}, \quad (3)$$

where $\alpha = 1/4$

$$c_{K+1}(x) = c_0(-x), \quad (4)$$

where the width of the basin is $2L$ ($-L \leq x \leq L$), and this is divided into $K + 1$ pieces, with $K + 2$ node points numbered from 0 to $K + 1$. Its x coordinate is denoted as x_k .

Table 2
Physical Parameters of Models 0, A, B, and C

| | First layer | Second Layer |
|-----------------------------|-----------------------|-----------------------|
| P -wave velocity α | 2.0 km/sec | 5.0 km/sec |
| S -wave velocity β | 1.0 km/sec | 2.5 km/sec |
| Density ρ | 1.2 g/cm ³ | 1.8 g/cm ³ |
| Q value | ∞ | ∞ |

Table 3
Conditions in Each Case in Numerical Experiments

| Case | Model | Angle | | No. of Obs. Point | Component of the Data |
|------|-------|----------|-----------|-------------------|-----------------------|
| | | θ | φ | | |
| A | A | 30° | 45° | 4 | x, y, z |
| B1a | B | 30° | 45° | 4 | x, y, z |
| B1b | | | 135° | | |
| B2 | | | 45&135° | | |
| C1 | C | 0° | 0° | 3 | x, y, z only y |
| C2 | | | | | |

In all cases, a time function of the incident wave is a Ricker wavelet with a characteristic period of 3 sec.

Figure 2 shows the spatial distribution of the function system $c_k(x)$ when $K = 8$. This function system is obtained by adding $c_0(x)$ and $c_{K+1}(x)$ to the function system used in Aoi *et al.* (1995). We add these two terms so that we can express the boundary shape with the minimum number of divisions, since the edge of basin is often steep. Except for the basin edge, the parameter p_k represents the difference in depth between the initial and the target models at x_k . The function system $c_k(x)$ is employed to give the depth at all points by interpolating these parameters.

Formulation of the Inversion

We denote the observation equation as

$$u_i(x_m, t_n; \mathbf{p}) = \tilde{u}_{i\text{inn}} \quad (\text{for all } i, m, n). \quad (5)$$

The model parameter \mathbf{p} has to satisfy equation (5) best in the sense of least square, where

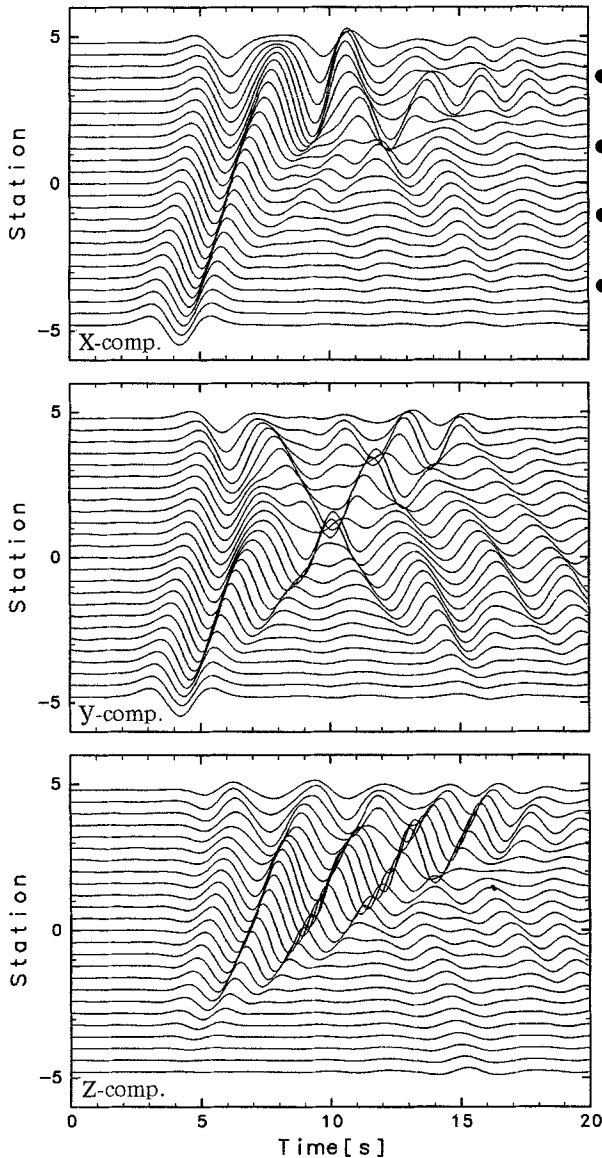


Figure 4. Seismograms recorded at surface stations located within the basin for model A. Incident wave is a Ricker wavelet with a characteristic period of 3 sec that impinges on the models with the incident angle $\theta = 30^\circ$ and the azimuth $\varphi = 45^\circ$. Only the waveforms from four stations indicated by \bullet are used for the inversion in case A. The shape of the underground structure is shown on the right of the top seismogram.

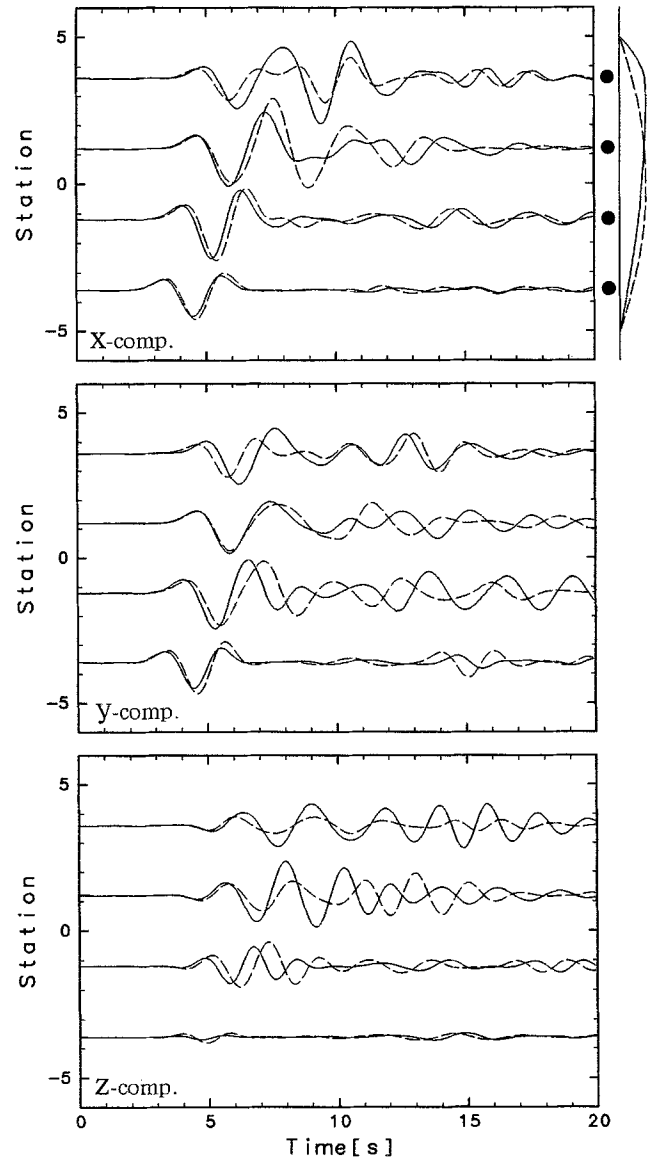


Figure 5. Waveforms from the four surface stations, indicated by \bullet in Figure 4, which are used for the inversion in case A (solid line), and the synthetic waveforms for the initial model, model 0, corresponding to the same four stations (broken line). The shape of the underground structure is shown on the right of the top seismogram.

$$\left\{ \begin{array}{l} u_i(x_m, t_n; \mathbf{p}): \text{synthetic waveform of } i\text{th component} \\ \quad \text{under a model parameter } \mathbf{p} \\ \tilde{u}_{i\text{mn}}: \text{observed waveform of } i\text{th component} \\ \quad \text{at } x_m \text{ and } t_n \text{ (given)} \\ x_m: m\text{th position} \\ t_n: n\text{th time sampling} \\ \mathbf{p}: \text{model parameter (vector)} \\ \quad (p_0, p_1, \dots, p_K, p_{K+1})^T \end{array} \right.$$

This observation equation being nonlinear, we obtain its solution by a linearized iterative method.

The left side of the observation equation is expanded in the Taylor series about the parameter \mathbf{p}^0 (the initial model) and is linearized by omitting the higher-order terms.

$$u_i(x_m, t_n; \mathbf{p}^0) + \sum_{k=1}^K \left. \frac{\partial u_i}{\partial p_k} \right|_{\mathbf{p}=\mathbf{p}^0} \delta p_k \approx \tilde{u}_{i\text{mn}}. \quad (6)$$

$\partial u_i / \partial p_k$ represents differential seismograms. Since they cannot be obtained analytically, they are replaced by finite-difference approximation.

$$\frac{\partial u_i}{\partial p_k} \approx \frac{u_i(x_m, t_n; \mathbf{p}^0 + \Delta \mathbf{p}_k) - u_i(x_m, t_n; \mathbf{p}^0)}{\Delta p_k}, \quad (7)$$

where Δp_k is an appropriate positive number,

$$\Delta \mathbf{p}_k = (0, \dots, \Delta p_k, \dots, 0)^T.$$

Equation (6) is a simultaneous linear equation with a non-square matrix as its coefficient. We solve this equation by

using a singular value decomposition method (e.g., Nakagawa and Oyanagi, 1982). We constrain the correction value for parameters in such a way that it becomes less than 50% of the depth at the corresponding point of the initial model for each iteration step; i.e.,

$$|\delta p_k| \leq 0.5 p_k^0 \quad (8)$$

for all k at all iteration steps. We construct the initial model for the next iteration step from this correction value for parameters thus calculated. We use the square sum of the residuals of data in order to judge the degree of convergence. Having performed the iteration by linearized iteration method until this square sum becomes sufficiently small, we consider this converged model as the finally estimated model.

Numerical Experiments of Inversion Method

We carry out various numerical experiments using different models and conditions. Boundary shapes of these basin structure models are shown in Figure 3. Table 1 shows the depths and the shapes of these models, and Table 2 shows their physical parameters. The conditions of the numerical experiments used for the following cases are summarized in Table 3.

Case A

Figure 4 shows synthesized waveforms on the surface when a plane SV wave [a Ricker wavelet (Ricker, 1977) with a characteristic period of 3 sec] impinges on model A (Fig.

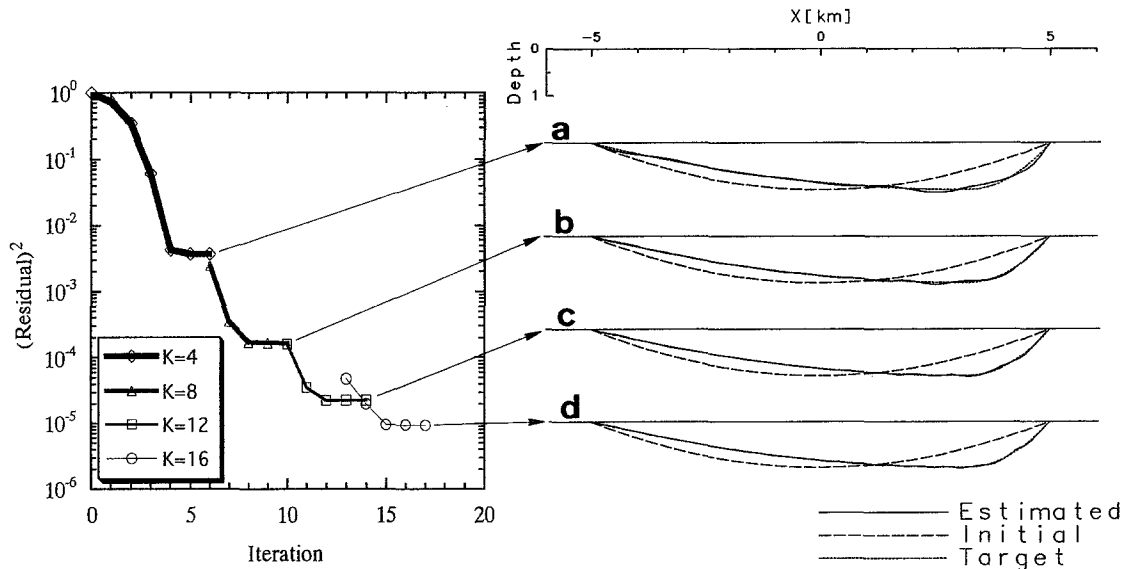


Figure 6. Change of the square sum of the residuals after each iteration and the estimated model for the inversion in case A. The residuals are normalized by that of the initial model. The number of parameters is increased by four each time the residuals converge. The initial (model 0), target (model A), and estimated models obtained at each step of the hierarchy are shown, respectively, by (a) through (d).

3 and Tables 1 and 2) with the incident angle $\theta = 30^\circ$ and the azimuth $\varphi = 45^\circ$ (Table 3). In all components, the arrival time of direct waves reflects the thickness of the sedimentary layer at each point, and these waves are followed by dominant surface waves, secondarily generated by the irregular structure, especially near the edges of the basin. The surface waves in the z component, which contain only Rayleigh waves, are not dominant in the shallow part near the left edge and become dominant as the basin gets deeper. With the x component, though the pattern is different, we can

observe a similar tendency. In contrast, as for the y component, the surface waves are generated similarly from both edges. Each component has thus a complex and different way to generate and propagate waves.

Among these waveforms, we take those at four stations on the surface within the basin, shown by \bullet , as our data and perform the inversion with model 0 (Fig. 3) as the initial model. The data (solid line) and the waveforms of model 0 at the corresponding four stations (broken line) are overlapping in Figure 5. The residuals of each iteration step and the

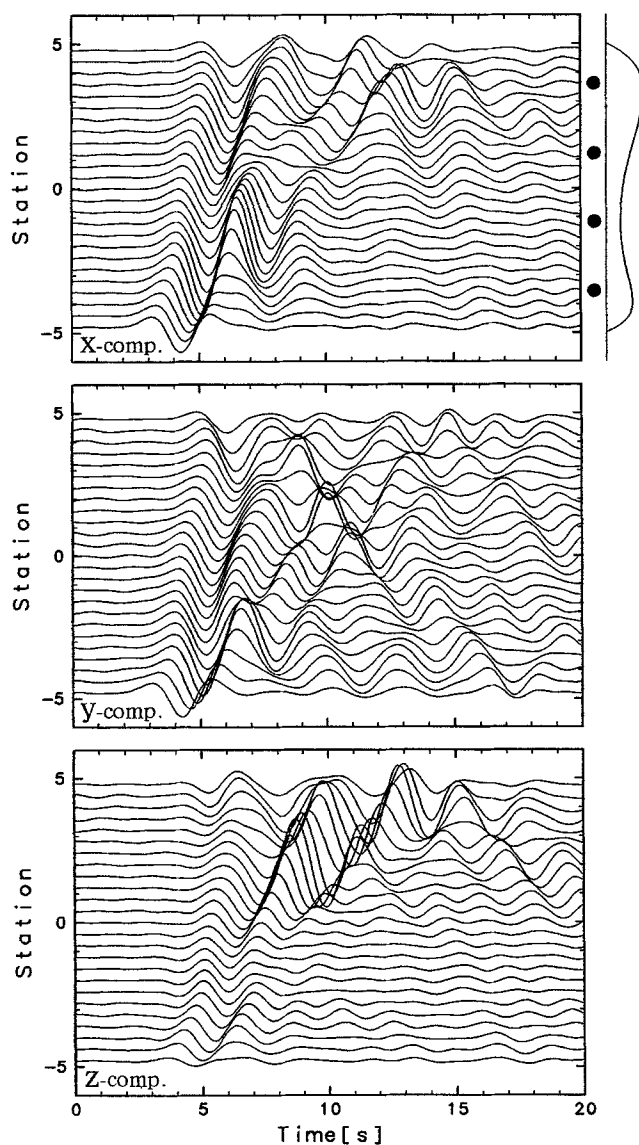


Figure 7. Seismograms recorded at surface stations located within the basin for model B. Incident wave is a Ricker wavelet with a characteristic period of 3 sec that impinges on the models with the incident angle $\theta = 30^\circ$ and the azimuth $\varphi = 45^\circ$. Only the waveforms from four stations shown by \bullet are used for the inversion in case B1a. The shape of the underground structure is shown on the right of the top seismogram.

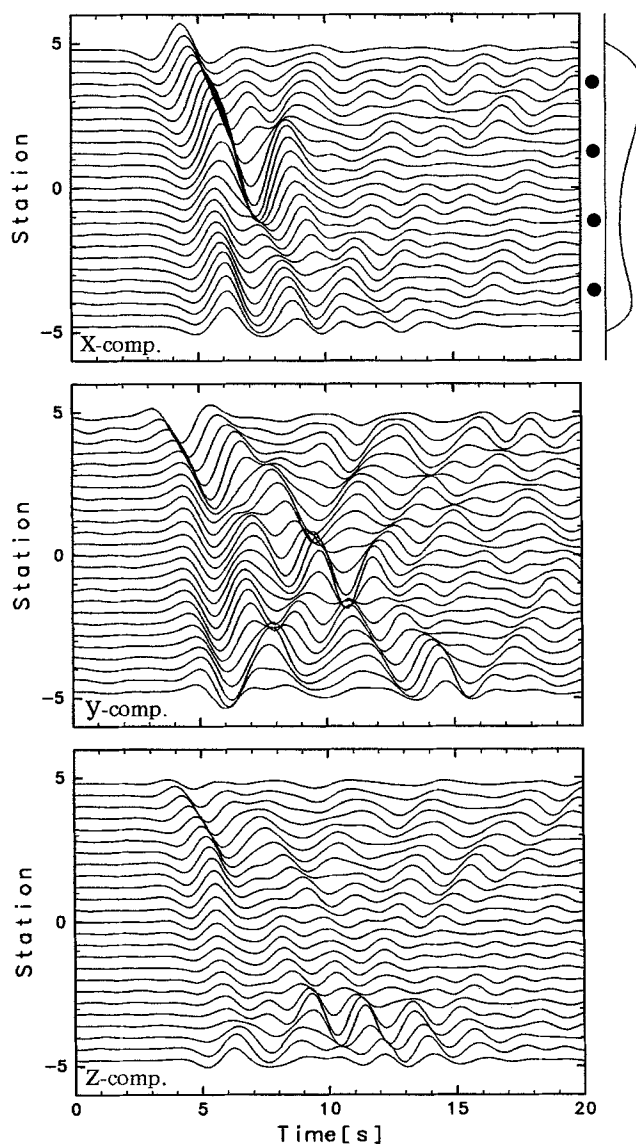


Figure 8. Seismograms recorded at surface stations located within the basin for model B. Incident wave is a Ricker wavelet with a characteristic period of 3 sec that impinges on the models with the incident angle $\theta = 30^\circ$ and the azimuth $\varphi = 135^\circ$. Only the waveforms from four stations shown by \bullet are used for the inversion in case B1b. The shape of the underground structure is shown on the right of the top seismogram.

estimated models in each hierarchical step are shown in Figure 6. First of all, we perform the inversion with $K = 4$. After the fifth iteration, where we can see the residuals becoming constant, the inversion is further performed with $K = 8$. In this way, K is increased to $K = 12$ and $K = 16$. We conclude that the model shown in Figure 6c is the ultimately estimated model from the fact that the residuals do not decrease any more when $K = 12$ is increased to $K = 16$. The result is already good when $K = 4$, and the final model (when $K = 16$) corresponds perfectly to the target model, model A, thus showing sufficient accuracy of the estimation of structure.

The Arrival Direction of the Incident Wave and the Estimated Model

Case B1

We carry out experiments with a more complex model, model B (Fig. 3 and Tables 1 and 2), which has a shallow part in the middle. Figure 7 shows the waveforms that we obtain when a plane SV wave (a Ricker wavelet with characteristic period of 3 sec) impinges on this model with the incident angle of $\theta = 30^\circ$ and the azimuth of $\varphi = 45^\circ$ (case B1a), and Figure 8 shows a case (case B1b) where the incident angle is $\theta = 30^\circ$ and the azimuth is $\varphi = 135^\circ$ (Table

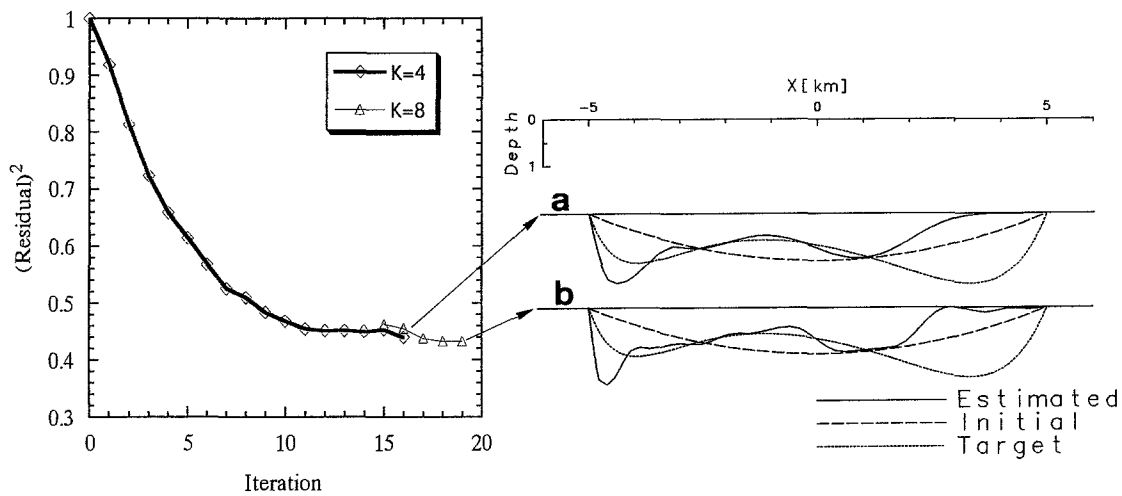


Figure 9. Change of the square sum of the residuals after each iteration and the estimated model for the inversion in case B1a. The residuals do not decrease sufficiently (note that the scale of the vertical axis is logarithmic), and only the left side of the structure is more or less correctly estimated.

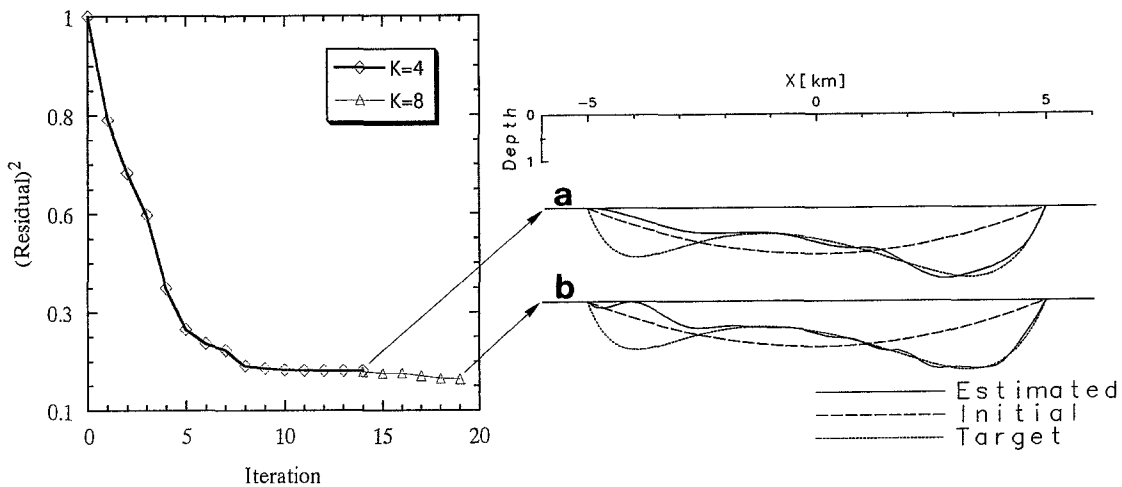


Figure 10. Change of the square sum of the residuals after each iteration and the estimated model for the inversion in case B1b. The residuals do not decrease sufficiently (note that the scale of the vertical axis is logarithmic), and only the right side of the structure is more or less correctly estimated.

3). The waveforms are more complex in model B than in model A, because the surface waves are generated secondarily by the irregular structure of the elevated part as well as by that near the edges. In case B1a, the surface waves secondarily generated from the right end of the elevated part and near the right edge of the basin get mixed. Therefore, there are many phases at the right side of the elevated part. On the contrary, in case B1b, the surface waves are dominantly generated, and many phases are observed at the left side of the elevated part. Among these waveforms, we take those at four stations on the surface within the basin, shown by ●, as our data and perform the inversion with model 0 as the initial model. The residuals of each iteration step and the estimated models in each hierarchical step from these inversions in cases B1a and B1b are respectively shown in Figures 9 and 10. In both cases, the residuals do not decrease sufficiently (note that the scale of the vertical axis is logarithmic), and the estimation of the structure is not precise. In fact, only the left side of the structure is more or less estimated correctly in case B1a, whereas only the right side is well estimated in case B1b.

The present method enables us to estimate the entire structure with data from a small number of surface stations because we use not only direct waves but also surface waves. The advantage of the use of the surface wave, which propagates horizontally with information about the structure underneath, is that it contains information covering a wider range of underground structure compared with the direct wave that has only information concerning the structure just underneath the observation stations. When the structures are complex as in case B1a or B1b, a complete inverse analysis

can be difficult because of the phases that overlap, even if we also use information from surface waves.

Case B2

As we examined in cases B1a and B1b, the estimation of the entire shape may not be possible when structures are too complex. Nevertheless, certain parts of the structure can be estimated correctly, and these parts that are possible to estimate are different according to the azimuth of the incident wave in each case. Therefore, in case B2 (Table 3), we perform an inversion using simultaneously two datasets of cases B1a and B1b from four surface stations within the basin indicated by ● in Figures 7 and 8. Figure 11 shows the residuals of each iteration step and the estimated models in each hierarchical step when we carry out the inversion. In this case, the residuals decrease sufficiently, and we are able to estimate the entire structure. As we have seen so far, there are certain parts that are difficult to estimate with the data from only one incident wave in cases of complex structure. In such cases, the simultaneous use of several waveforms from different incident directions enables us to estimate the entire structure with waveforms from a small number of observation stations.

Through the numerical experiments, we are able to find out the appropriate locations of observation stations or the arrival direction of incident wave, which are necessary to perform an accurate inverse analysis. In cases where the data are insufficient, we are also able to tell which part of the estimated structure can be trusted. Therefore, we should choose this part of the structure as the target of our analysis with a given dataset.

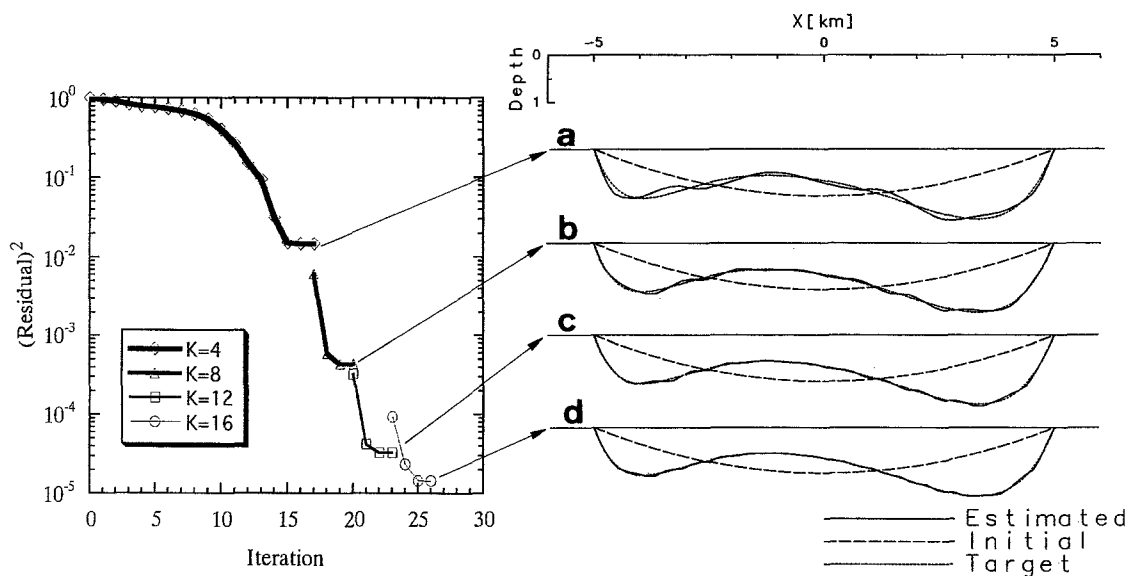


Figure 11. Change of the square sum of the residuals after each iteration and the estimated model for the inversion in case B2. The simultaneous use of two waveforms (cases B1a and B1b) enables us to estimate the entire structure.

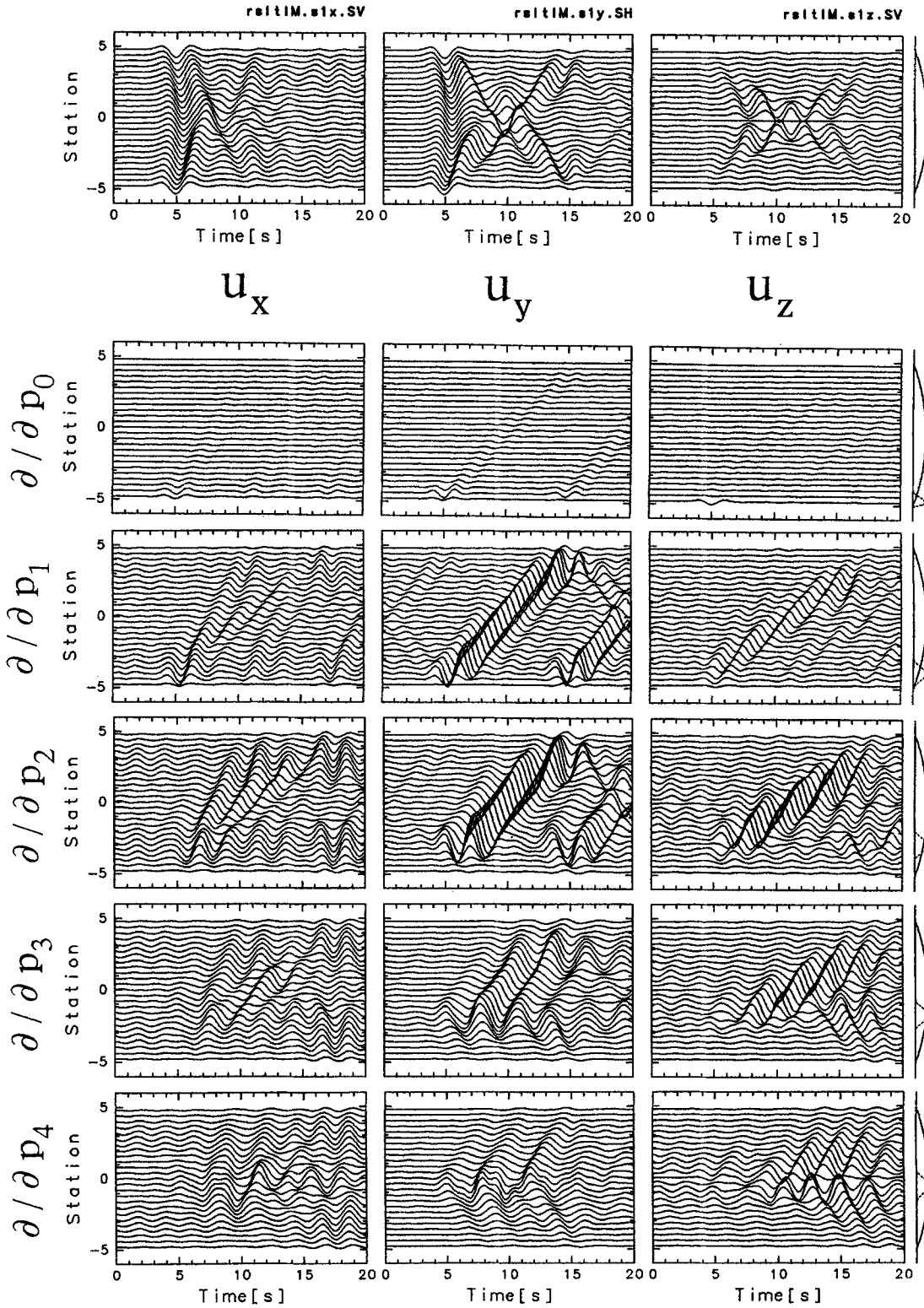


Figure 12. Seismograms u_i and the corresponding differential seismograms $\Delta u_i / \Delta p_k$. The top row shows the seismograms produced by a Ricker wavelet with a characteristic period of 3 sec that impinges on model 0 vertically from below. The second to the sixth rows show, respectively, the differential seismograms $\Delta u_i / \Delta p_k$ of model 0 for $K = 8$ that correspond to $k = 0$ through 4. For each $\Delta u_i / \Delta p_k$, the shape of the functions $c_k(x)$, which is corresponding to the parameter p_k with respect to which the seismogram u_i is differentiated, is indicated by broken lines with the basin models (solid line), at the right side of the figure.

Discussion

Differential Seismograms

We show that three components of differential seismograms have different time and space distributions in the simple 2D case. The top row of Figure 12 shows the seismograms u_i produced by a Ricker wavelet with a characteristic period of 3 sec that impinges on model 0 vertically from below. u_x and u_z show, respectively, waveforms of radial and z components when an SV wave impinges, and u_y indicates a waveform of transverse component when an SH wave impinges. The second row through the sixth row are differential seismograms $\Delta u_i / \Delta p_k$ when $K = 8$, each row corresponding to $k = 0$ through 4. For each $\Delta u_i / \Delta p_k$, the functions $c_k(x)$ corresponding to the parameters p_k , with respect to which the seismogram u_i is differentiated, are indicated by broken lines with the basin models, at the right side of the figure.

For all k , the following two parts are manifestly dominant in the differential seismograms $\Delta u_x / \Delta p_k$ and $\Delta u_y / \Delta p_k$. One of them is the direct wave observed in places where $c_k(x)$ is not zero. The basis function $c_k(x)$ corresponds to the parameter p_k , with which the waveform, u_x or u_y , is differentiated. The other dominant part consists of the surface waves that propagate from this direct wave part. This char-

acteristic becomes more evident in the differential seismograms corresponding to the parameter near the edge ($k = 1, 2$). However, differential seismograms corresponding to the parameter p_0 do not have large amplitude because the sedimentary layer is very shallow close to the edge (around x_0), and the surface waves are not generated there. As we have seen, in spite of the common characteristic explained above, the time and space distributions and the amplitude are very different in each component.

Condition Number of Linearized Equation

Since differential seismograms show different patterns for three components, we can imagine that the inversion with three components is more advantageous than the inversion with only one of them. We demonstrate this by examining the condition number of the linearized equation (6).

The condition number κ , which is a quantity related to the propagation law of errors in the equation (e.g., Nakagawa and Oyanagi, 1982), is defined as $\kappa = \mu_1 / \mu_m$. μ_1 and μ_m denote, respectively, the maximum and minimum singular values of the coefficient matrix of the linearized equation. The relative error of the solution is known to be smaller than that of the data multiplied by κ . Because of noise in data or errors generated by linearized approximation in nonlinear

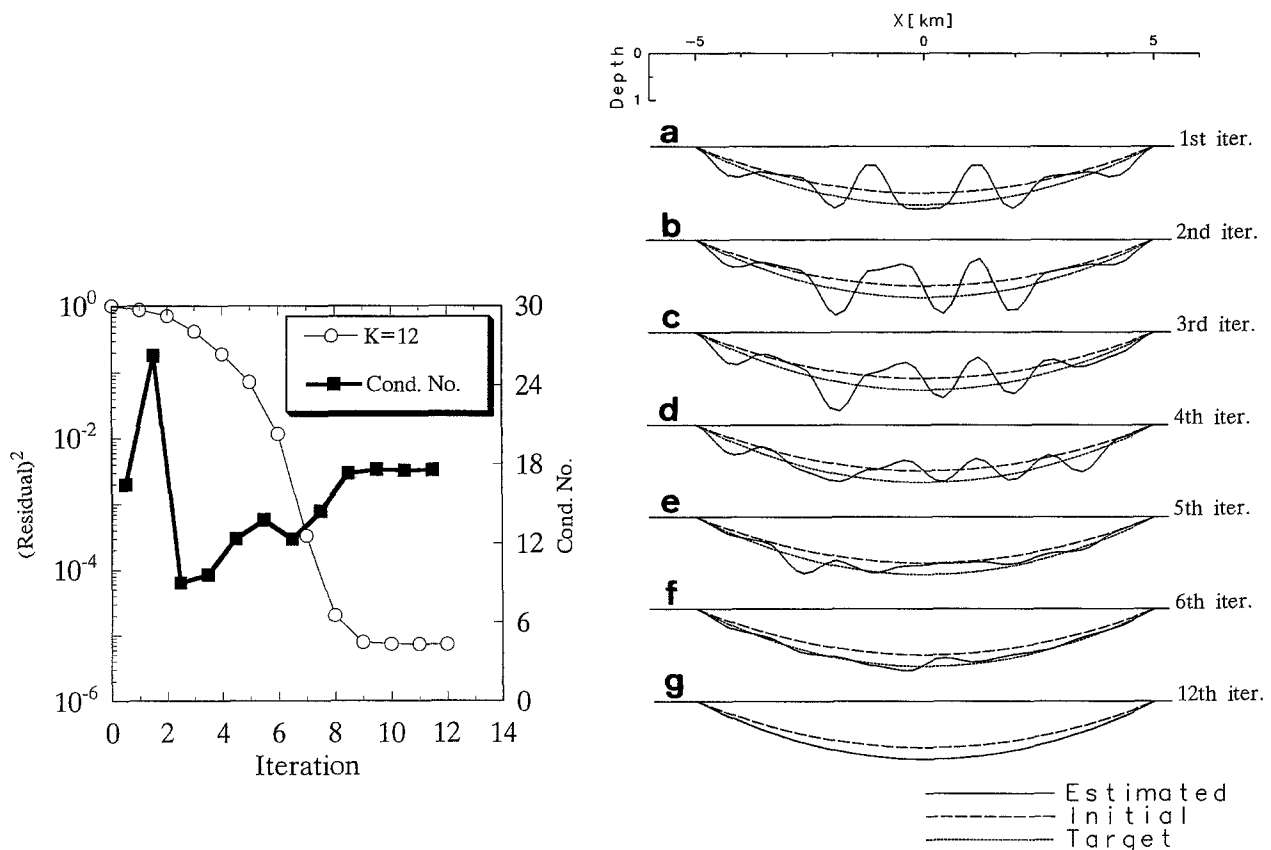


Figure 13. Change of the square sum of the residuals and condition number after each iteration and the estimated model for the inversion with only one component (transverse component).

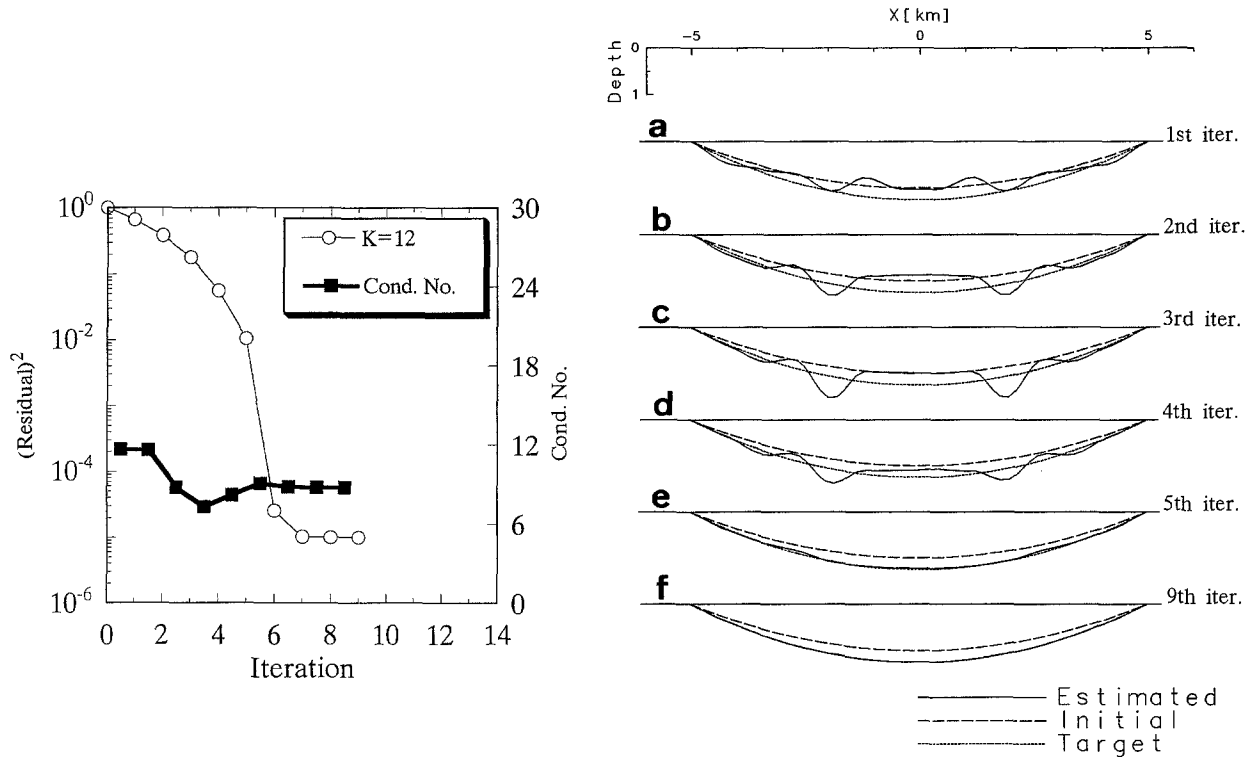


Figure 14. Change of the square sum of the residuals and condition number after each iteration and the estimated model for the inversion with three components.

problems, it is important to have a small condition number in order to perform a stable inversion.

Case C

Here we compare the inversion using three components with that using only one component in a simple 2D problem where the azimuth and incident angle are both 0° (vertical incidence). We perform the inversion with model C (Fig. 3 and Tables 1 and 2) as the target model and model 0 as the initial model. In this case, we do not impose the constraint, equation (8), to achieve a stable computation that we imposed to solve the linearized equation (6), since the purpose is to examine the process of each inversion. The residuals and the estimated models in each iteration step of the inversion with only one component (*SH* component) are shown in Figure 13 (case C1), and case C2 with both *P-SV* and *SH* components is shown in Figure 14 (Table 3). Comparing these results, we can see that the condition number is smaller and the convergence is more rapidly achieved in the latter. We also know that although the final estimation is correct in both cases, it is more unstable to process the inversion in the case with only one component. Therefore, we conclude that the use of three components allows us to estimate the basin structure with increased accuracy and speed of convergence.

Conclusions

We extended our new waveform inversion method with boundary shape as its target to cases where the plane wave with an arbitrary azimuth impinges on the 2D structure and carried out numerical experiments.

Even if the structure is 2D, this cannot be treated as a simple 2D problem because of the wave with an azimuth that is not 0° . Therefore, we treated it as a so-called 2.5D problem of boundary integral equation method so that we can perform the inversion for plane waves with an arbitrary azimuth. Such an expansion enabled us

- to perform the inversion also in cases where the epicenter has any azimuth to the structure and
- to perform a more stable inversion compared to an inversion with only the *SH* component since we can use waveforms of three components as data.

The latter was demonstrated through the facts that the three components in the differential seismograms, which are the kernels of the inversion, have different patterns; that the condition number of the linearized equation is smaller; and that the numerical experiments provide a stable process.

Using numerical experiments, we also showed that certain parts in the structure are easier to estimate than others,

and it depends on the arrival direction of the incident wave. We demonstrated that in such a case, we can estimate the entire structure by using simultaneously the data from incident waves from several directions.

The numerical experiments showed us that the extension of the present inversion scheme to cases where plane waves with an arbitrary azimuth impinge on the structure leads us to an estimation with increased accuracy and rapidity of convergence under more general conditions of the epicenter locations.

Acknowledgments

We thank Hiroshi Takenaka and Francisco J. Sánchez-Sesma for their most helpful suggestions. Computation time was provided by the Super-computer Laboratory, Institute for Chemical Research, Kyoto University. This work was partially supported by Grants-in-Aid for Scientific Research from the Ministry of Education, Science, and Culture of Japan (05302069). We would also like to show our gratitude for Prof. Campillo and an anonymous referee that helped us revise this article.

References

- Aoi, S., T. Iwata, K. Irikura, and F. J. Sánchez-Sesma (1995). Waveform inversion for determining the boundary shape of a basin structure, *Bull. Seism. Soc. Am.* **85**, 1445–1455.
- Barone, M. R. and D. A. Caulk (1982). Optimal arrangement of holes in a two-dimensional heat conductor by a special boundary integral method, *Int. J. Num. Meth. Eng.* **18**, 675–685.
- Beck, J. L. and J. F. Hall (1986). Factors contributing to the catastrophe in Mexico City during the earthquake of September 19 1985, *Geophys. Res. Lett.* **13**, 593–596.
- Fujiwara, H. (1996). Three-dimensional wavefield in a two-dimensional basin structure due to point source, *J. Phys. Earth* **44**, 1–22.
- Hatayama, K., K. Matsunami, T. Iwata, and K. Irikura (1995). Basin-induced Love waves in the eastern part of the Osaka basin, *J. Phys. Earth* **43**, 131–155.
- Kawase, H. and K. Aki (1989). A study on the response of a soft basin for incident S, P, and Rayleigh waves with special reference to the long duration observed in Mexico City, *Bull. Seism. Soc. Am.* **79**, 1361–1382.
- Kubo, S. (1992). *Inverse Problems*, Baifukan, Tokyo (in Japanese).
- Kubo, S., T. Sakagami, K. Ohji, T. Hashimoto, and Y. Matsumuro (1988). Quantitative measurement of three-dimensional surface cracks by the electric potential CT method, *J. Mech. Soc. Japan A* **54**, 218–225 (in Japanese with English abstract).
- Nakagawa, T. and Y. Oyanagi (1982). *Experimental Data Analysis by the Least-Squares Method*, Univ. of Tokyo Press, Tokyo (in Japanese).
- Nishimura, N. and S. Kobayashi (1991). A boundary integral equation method for an inverse problem related to crack detection, *Int. J. Num. Meth. Eng.* **32**, 1371–1387.
- Nowack, R. L. and L. W. Braile (1993). Refraction and wide-angle reflection tomography: theory and results, *Seismic Tomography: Theory and Practice*, 733–763.
- Pedersen, H. A., M. Campillo, and F. J. Sánchez-Sesma (1995). Azimuth dependent wave amplification in alluvial valleys, *Soil Dyn. Earthquake Eng.* **14**, 289–300.
- Pei, D. and A. S. Papageorgiou (1993). Study of the response of cylindrical alluvial valleys of arbitrary cross-section to obliquely incident seismic waves using the discrete wave number boundary element method, in *Soil Dynamics and Earthquake Engineering VI*, A. S. Cakmak, and C. A. Brebbia (Editors), Comp. Mech. Publications—Elsevier Appl. Sc., Southampton-London, pp. 149–161.
- Ricker, N. H. (1977). *Transient waves in visco-elastic media*, Elsevier Scientific Publishing Co., Amsterdam.
- Tanaka, M. and K. Yamagiwa (1988). Application of boundary element method to some inverse problems in elastodynamics, *J. Mech. Soc. Japan A* **54**, 1054–1060 (in Japanese with English abstract).
- White, D. J. (1989). Two-dimensional seismic refraction tomography, *Geophys. J.* **97**, 223–245.
- Yamanaka, H., K. Seo, and T. Samano (1989). Effects of sedimentary layers on surface-wave propagation, *Bull. Seism. Soc. Am.* **79**, 631–644.

Disaster Prevention Research Institute
Kyoto University
Gokasho, Uji City
Kyoto 611, Japan
aoi@geo.bosai.go.jp
(S.A., T.I., K.I.)

National Research Institute for Earth Science and Disaster Prevention
3-1 Tennodai, Tsukuba
Ibaragi, 305 Japan
(S.A., F.H.)

Manuscript received 13 February 1996.